Monitoring of apoptosis of HL60 cells by Fourier-transform infrared spectroscopy

Fabio GASPARRI*† and Marta MUZIO*[1]

*DRO-Oncology, Pharmacology Department, Pharmacia Corp., Via Pasteur 10, 20014 Nerviano, Italy, and †Department of Biotechnology and Bioscience, University of Milano-Bicocca, Piazza della Scienza 2, 20126, Milano, Italy

Fourier-transform infrared (FTIR) spectroscopy is a vibrational technique that gives information on the chemical composition of a sample, providing a 'molecular fingerprint' of it. It is a powerful approach to study intact cells. The aim of the present study was to analyse and quantify apoptotic cells by using a FTIR approach based on attenuated total reflection (ATR). We incubated human HL60 leukaemic cells with camptothecin, a cytotoxic drug, and monitored apoptosis induction over a period of time. Several ATR–FTIR spectral changes occurred during the apoptotic process. In particular, we observed that the apoptotic index was inversely correlated with the spectral area in the region 1200–900 cm^{-1}, assigned to the absorption of nucleic acids. We therefore propose that ATR–FTIR spectral features may be used as a diagnostic marker of apoptotic cells.

Key words: attenuated total reflection, camptothecin, necrosis.

INTRODUCTION

Apoptosis, or programmed cell death, is characterized by typical morphological and metabolic changes: cells undergoing apoptosis shrink, their DNA is cleaved into regular fragments, and their nuclei condense [1]. This process requires sequential activation of cysteine proteases belonging to the caspase family. Caspase activation triggers a cascade of signalling mediators, which eventually results in phosphatidylserine exposure on the cell surface, chromatin condensation and genomic DNA cleavage.

At present, detection of apoptotic cells can be performed by several assays that analyse either morphological changes or distinct biochemical events occurring during programmed cell death. Methods for the latter include nuclear morphological analysis, cleavage assays of specific caspase substrates [2], detection of phosphatidylserine externalization by annexin V (Anx V) staining [3], analysis of DNA fragmentation by gel electrophoresis [4] and terminal deoxynucleotidyltransferase-mediated dUTP nick end labelling ('TUNEL') [5]. All of these methods require sample handling and staining. Furthermore, they provide information on one single effect of apoptosis, but none of these assays provides a global view on the biochemical status of an apoptotic cell. The execution of each apoptotic event is defined chronologically with respect to another. For some assays, positively identified cells appear earlier than other apoptotic features, whereas in other assays the positive signals occur only late in the process [6,7]. This could lead to some inconsistencies when assessing the apoptotic index by using different assays.

Fourier-transform infrared (FTIR) spectroscopy is a vibrational technique that gives information on the chemical composition of a given sample [8]. This technique presents several advantages, such as sensitivity, rapidity and no requirement for staining or reagents. During the last decade, FTIR spectroscopy has proven to be a powerful tool for the study of biological fluids, isolated cellular components and even intact cells and tissues [9]. The ability of FTIR spectroscopy to detect changes in the chemical composition and morphology of intact cells led to its use in distinguishing differences among cell populations; for example, between normal and tumoral cells [10–12].

Among the methods used for acquiring IR spectra of biological samples, attenuated total reflection (ATR) is one of the most powerful. The band shape in an ATR–FTIR spectrum depends on the wavelength of the incidence radiation, on the angle of incidence and on the refractive index of both the internal reflection element and the sample [13]. The ATR technique has distinct advantages over transmission. For example, problems resulting from light scattering or signal saturation are virtually absent, and the optical-path length is consistent and well defined, depending only on the geometry of the internal reflection element [13]. Given these characteristics, this technique can be considered to be broadly accessible and highly reproducible. Transmission FTIR spectroscopy, but not ATR–FTIR spectroscopy, was recently applied to detect changes occurring during differentiation and apoptosis of leukaemic cell lines; however, the results were contradictory and not conclusive. In particular, Wang and co-workers [14] found that the absorption in the spectral region assigned to nucleic acids increased following apoptosis. In contrast, Mantsch's group, by using a different experimental system, observed a decrease in the same region [15].

The aim of the present study was to investigate the possibility of using an FTIR spectroscopic approach based on ATR for the analysis and quantification of apoptosis. Here, we compared ATR–FTIR spectra of HL60 (human promyelocytic leukaemia) cells after induction of apoptosis with those of either viable growing or necrotic HL60 cells. We observed a direct correlation between the FTIR spectral changes of HL60 cells undergoing cell death and the apoptotic index in a time- and dose-dependent manner; these observations were confirmed by two standard methods. We therefore suggest that ATR–FTIR spectroscopy

Abbreviations used: Anx V, annexin V; ATR, attenuated total reflection; DAPI, 4,6-diamidino-2-phenylindole; FTIR, Fourier-transform infrared; PARP, poly(ADP-ribose) polymerase; PI, propidium iodide; Z-VAD-fmk, benzyloxycarbonyl-valylalanyl-DL-aspartylfluoromethane.

[1] To whom correspondence should be addressed (e-mail marta.muzio@pharmacia.com).

may be used for the analysis and quantification of apoptotic cells.

EXPERIMENTAL

Cellular cultures

HL60 cells, obtained from the European Collection of Animal Cell Cultures (ECACC; Salisbury, Wilts., U.K.), were grown as a suspension in RPMI 1640 medium (Gibco BRL, Gaithersburg, MD, U.S.A.) containing 2 g/l D-glucose, supplemented with 10 % (v/v) heat-inactivated fetal bovine serum (Gibco BRL), L-glutamine (2 mM), penicillin (100 units/ml) and streptomycin (100 mg/ml). Cells were maintained at 37 °C in a humidified atmosphere with 5 % CO_2. Cellular size and concentrations were determined by means of a Coulter Counter Multisizer II [Instrumentation Laboratory Company (IL Instruments), Lexington, KY, U.S.A.].

Apoptosis and necrosis induction

Apoptosis was induced by treating the cells for different times with camptothecin, a well-characterized cytotoxic alkaloid topoisomerase I inhibitor [16–18]; apoptosis induction was then confirmed by two different standard methods. First, cells were stained by 4,6-diamidino-2-phenylindole (DAPI; Boehringer, Mannheim, Germany) and scored as apoptotic by nuclear morphological analysis. At least 200 cells were counted in each sample. Fluorescence photomicrographs of normal and apoptotic cells were obtained by means of a fluorescence microscope DMRB (Leica Microsystems, Mannheim, Germany) equipped with a charge-coupled-device ('CCD') camera VarioCam (PCO Computer Optics, Kelheim, Germany). Alternatively, cells were stained with Anx V–FITC/propidium iodide (PI) (Annexin V-FITC Apoptosis Detection Kit, Beckton Dickinson, San Jose, CA, U.S.A.), and analysed by flow cytometry using a FACScan equipped with a Xe/Ne laser at 488 nm (Beckton Dickinson). Viable cells are double-negative; early apoptotic cells are Anx V-positive, but PI-negative; late apoptotic and necrotic cells are Anx V-positive and PI-positive [3]. The apoptotic index was calculated as the sum of early and late apoptotic cells divided for the total number of events. The caspase inhibitor benzyloxycarbonyl-valylalanyl-DL-aspartylfluoromethane (Z-VAD-fmk) was obtained from Bachem AG (Bubendorf, Switzerland).

Two methods for inducing necrosis were used: heat and oxidative shock. Cells induced in necrosis by heat were resuspended in 0.9 % (w/v) NaCl sterile solution and incubated for 3 h at 55 °C, as described previously [19]. Alternatively, cells were suspended in 0.9 % NaCl solution containing 1 % H_2O_2 and incubated for 3 h at room temperature (approx. 23 °C). Cell lysis was confirmed by morphological analysis and Anx V–FITC/PI staining, as described above.

Western blot analysis

HL60 cells were lysed in a buffer containing 50 mM Tris/HCl, pH 7.4, 150 mM NaCl, 1 mM EDTA, 0.2 % (v/v) Nonidet P40 and protease inhibitor cocktail (Roche, Zurich, Switzerland) on ice for 10 min. Cell debris was pelleted by centrifugation, and the total protein concentration of the soluble extracts was determined by the Bradford assay, according to the manufacturer's instructions (Bio-Rad, Munich, Germany). Total soluble protein extract (30 μg) for each sample was resolved by SDS/PAGE (12 % gels). After electrophoresis, the proteins were transferred to nitrocellulose, and the blot was blocked for 1 h at room temperature with a solution of 5 % dried milk in PBST [0.1 % (v/v) Tween 20 in PBS]. The blot was incubated with anti-(caspase-3) primary antibody (BD Pharmingen, San Diego, CA, U.S.A.) or anti-[poly (ADP-ribose) polymerase] (PARP) primary antibody (Oncogene, Cambridge, MA, U.S.A.) in blocking solution at 4 °C overnight. Primary antibodies were detected using a horseradish-peroxidase-conjugated secondary antibody (Amersham Biosciences, Little Chalfont, Bucks., U.K.) and enhanced chemiluminescence as described by the manufacturer (Chemiluminescent Substrate Super Signal; Pierce, Rockford, IL, U.S.A.).

Sample preparation for ATR–FTIR spectroscopy

Since the degree of hydration strongly affects FTIR spectral features of major cellular components [20,21], cells were measured as dehydrated Bio-film: this practice allows reliable absorption spectra in the region 700–4000 cm^{-1} to be obtained. Cells [$(2–4) \times 10^6$] were collected by centrifugation at 4 °C and washed once with sterile 0.9 % NaCl solution. The pellet was suspended in 300 μl of 0.9 % NaCl solution, and then spread uniformly on the surface of the internal reflection element for ATR measurements. Cells were then dried at room temperature under airflow for 15 min, and analysed without any further manipulation or staining.

ATR–FTIR spectroscopy

All ATR–FTIR absorption spectra were recorded at room temperature in the range 700–4000 cm^{-1} with a spectrometer Spectrum 1000 (PerkinElmer) equipped with a deuterated triglycine sulphate ('DTGS') detector. The horizontal ATR accessory used was a ZnSe crystal with an incidence angle of 45° (PerkinElmer). For each spectrum, 64 interferograms were co-added, and these were averaged at a nominal spectral resolution of 2 cm^{-1} and at a sampling interval of 1 cm^{-1}. No smoothing, correction for atmospheric water background or correction for the dependence of the penetration depth on the wavelength were performed on the original ATR–FTIR spectra. All the spectral area integrations and calculations were performed by an Excel macro (Microsoft, U.S.A.) developed by the authors. In order to enhance the fine spectral structure, some representative spectra were analysed by deriving second derivatives. These spectra were smoothed previously to reduce noise background (13 points; after Savitzky and Golay [22]), and second derivatives of the smoothed spectra were calculated using Spectrum v2.00 software (PerkinElmer).

RESULTS AND DISCUSSION

Spectral analysis of apoptotic and necrotic HL60 cells

HL60 cells were treated with either the cytotoxic drug camptothecin to induce apoptosis, or with H_2O_2 and heat to induce necrosis. The FTIR spectra of viable, apoptotic or necrotic cells were analysed: viable HL60 cells gave typical IR spectra of leukaemic cells, as described previously ([23,24]; also see Figure 1). Infrared spectra of apoptotic HL60 cells were acquired following treatment with 4 μM camptothecin for 20 h; FTIR spectra of necrotic HL60 cells were obtained following heat shock or oxidative stress (see the Experimental section). Induction of apoptosis or necrosis was confirmed by flow cytometry (71 % and 99 % cell death respectively; results not shown).

Representative IR absorption spectra acquired in the region 700–4000 cm^{-1} are shown in Figure 1. ATR–FTIR spectra of viable, apoptotic and necrotic HL60 cells are dominated by two

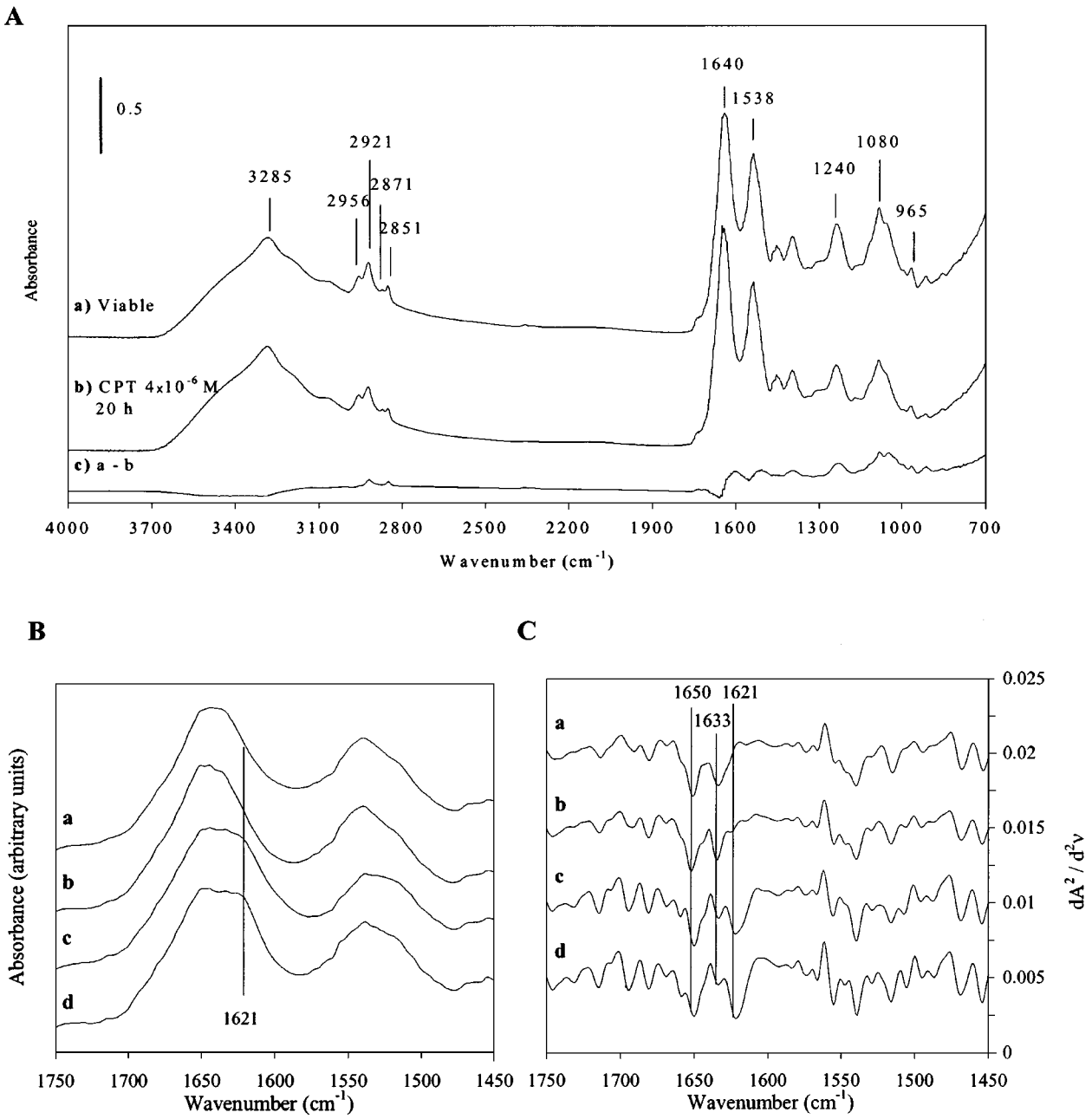

Figure 1 ATR–FTIR spectra of viable, apoptotic and necrotic HL60 cells

(**A**) Region 700–4000 cm^{-1} of the ATR–FTIR absorption spectra of viable (spectrum **a**) and apoptotic (spectrum **b**) HL60 cells. Apoptosis was induced by treating the cells with 4 μM camptothecin (CPT) for 20 h and confirmed by FACS analysis (Anx V–FITC/PI staining; 71% apoptosis). In order to emphasize the differences between spectrum (**a**) and spectrum (**b**), the difference spectrum (**c**) is also shown. (**B**) Region 1450–1750 cm^{-1} of the ATR–FTIR spectra of viable (**a**), apoptotic (**b**) and necrotic (**c** and **d**) HL60 cells. Necrosis was induced by treating cells with H_2O_2 (spectrum **c**) or by heat shock (spectrum **d**), and confirmed by FACS analysis (Anx V–FITC/PI staining; 99% necrosis). (**C**) Second-derivative spectra corresponding to (**B**), as obtained after smoothing of the original spectra (as described by Savitzky and Golay [22]; 13 points).

bands assigned to the absorption modes of proteins: the most intense is the amide I band, centred near 1640 cm^{-1}, which corresponds to the C=O stretching coupled to the N–H bending and the C–N stretching modes of peptidic bonds [23,24]. It has been reported previously that the shape of the amide I band is influenced by the overall secondary structure of cellular proteins. In particular, the peaks assigned to α-helices, β-sheets, turns and random coil have absorption maxima between 1645–1662 cm^{-1}, 1613–1637 cm^{-1}, 1662–1682 cm^{-1} and 1637–1645 cm^{-1} respectively [25]. The amide II band at 1538 cm^{-1} arises from vibrational modes that involve the C–N–H bending and C–N stretching of peptidic bonds [26].

Spectral analysis showed some major differences between viable and apoptotic cells. Spectra of apoptotic cells show a significant intensity decrease in the region between 900 and 1300 cm^{-1}, with respect to viable cells (Figure 1A). The complex band pattern in this range represents the superimposed contributions of nucleic acids (DNA, RNA), carbohydrates and phos-

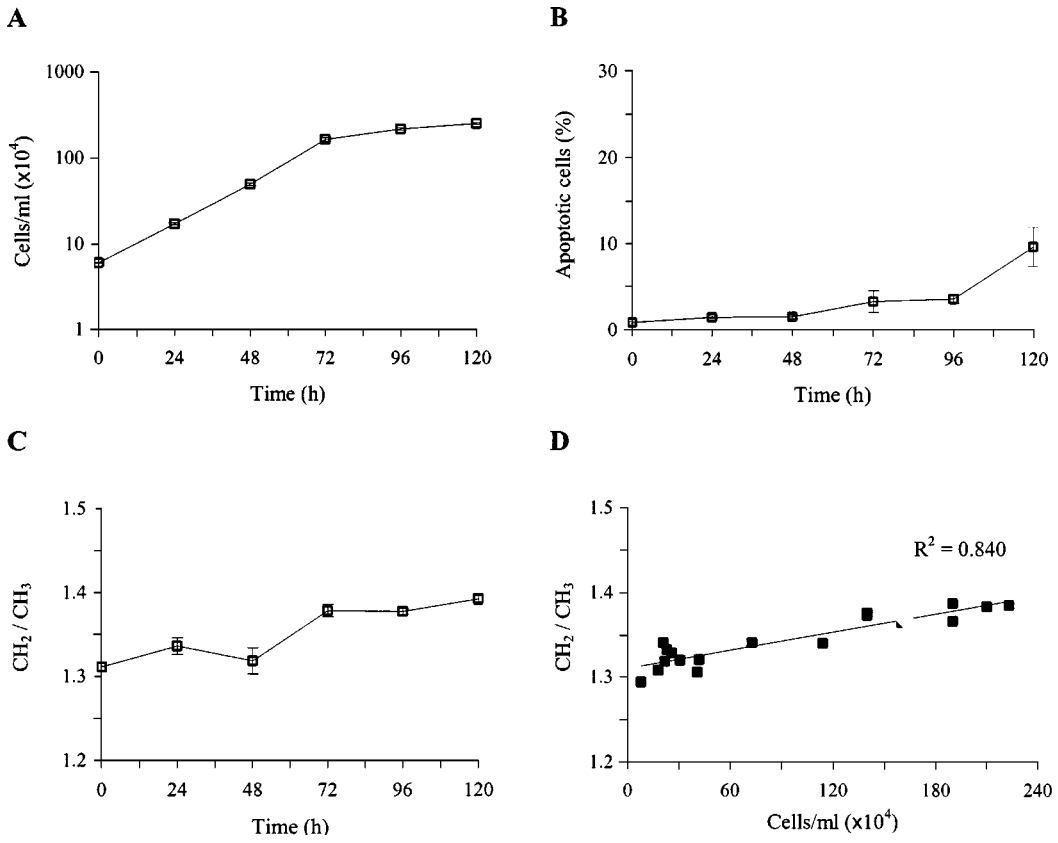

Figure 2 Increase of the CH_2/CH_3 ratio during normal cell growth

(**A**) Growth curve of HL60 cells (values plotted are the means from three independent experiments). (**B**) Apoptotic index of growing cells was assessed by nuclear morphology analysis and scoring (cells correspond to the experiment shown in **A**). (**C**) Time-course analysis of the CH_2/CH_3 ratio during cell growth (mean values $\pm$ S.D. for three independent experiments). (**D**) Statistical correlation between the CH_2/CH_3 ratio and the cell number in independent cultures. Each single point represents a different HL60 culture.

phates [9]. In particular, the band centred at 1080 cm^{-1} is assigned to the symmetric stretching mode of phosphodiester bonds ($\nu_s PO_2^-$) in nucleic acids, whereas the band at 1240 cm^{-1} originates from asymmetric PO_2^- stretching ($\nu_{as} PO_2^-$) [27]. The peak at 965 cm^{-1} arises from a C–C stretching mode of (deoxy)ribose that is present in DNA and RNA [27]. As shown in Figure 1(A), the overall intensity of the region assigned to nucleic acids significantly decreases compared with the amide bands following apoptosis. The area between 1000–1140 cm^{-1} shows the most prominent differences, and was analysed further as a marker of apoptosis (see Figures 3–6 and below).

The second significant difference was observed in the ratio between the band areas of amide I (1599–1710 cm^{-1}) and amide II (1483–1595 cm^{-1}). The amide I/amide II ratio increased from 1.068 ± 0.016 in normal cells (means $\pm$ S.D. for 15 independent samples) to 1.117 ± 0.022 in apoptotic cells (means $\pm$ S.D. for 11 independent samples; Figure 1A). These data suggest that overall biochemical and biophysical changes of cellular proteins occur following apoptosis. We hypothesize that cleavage of cellular proteins performed by distinct apoptotic caspases ([19,28]; also see Figure 6), the modulation of chaperone activity [29,30] and proteasome function [31], or the cytoplasmic acidification [32] occurring during apoptosis could affect the overall protein folding and localization, and therefore also the IR absorption of peptidic bonds.

Apoptotic HL60 cells show a slight overall absorption decrease of the region between 2800 and 3000 cm^{-1} compared with normal cells (Figure 1A). This region is dominated by the absorption modes of aliphatic chains (mainly phospholipids and fatty acids). In particular, the bands at 2956 cm^{-1} and 2871 cm^{-1} originate, respectively, from the asymmetric stretching ($\nu_{as} CH_3$) and the symmetric stretching ($\nu_s CH_3$) of CH_3 groups. The band at 2921 cm^{-1} is assigned to the asymmetric stretching of CH_2 ($\nu_{as} CH_2$); the band at 2851 cm^{-1} is assigned to the symmetric stretching of CH_2 groups ($\nu_s CH_2$) [33].

The spectra of viable growing, apoptotic and necrotic cells were compared. Necrosis was induced by heat shock (55 °C, 3 h) or by oxidative stress (3 h treatment with 1 % H_2O_2). The overall spectral changes that were observed previously with apoptotic cells also appeared during necrosis, with a notable exception. A marked shoulder in the amide I band appeared at approx. 1621 cm^{-1} in necrotic cells, compared with either normal or apoptotic cells (Figure 1B). In order to enhance the fine spectral structure, the spectra within this region were smoothed (see the Experimental section) and second derivatives were calculated (Figure 1C). A novel band centred at 1621 cm^{-1} appeared within necrotic cells only. Significantly, this is a spectral feature observed in necrotic cells induced by either heat shock or oxidative damage. On the other hand, the frequencies of the maximum of the peaks centred at 1650 cm^{-1} (assigned to α-helix) and 1633 cm^{-1} (assigned to β-sheets) are not affected in either apoptotic or necrotic cells, supporting further the specificity of the observed effects. Given these observations, we propose that the 1621 cm^{-1} band may be used as a spectral marker that allows

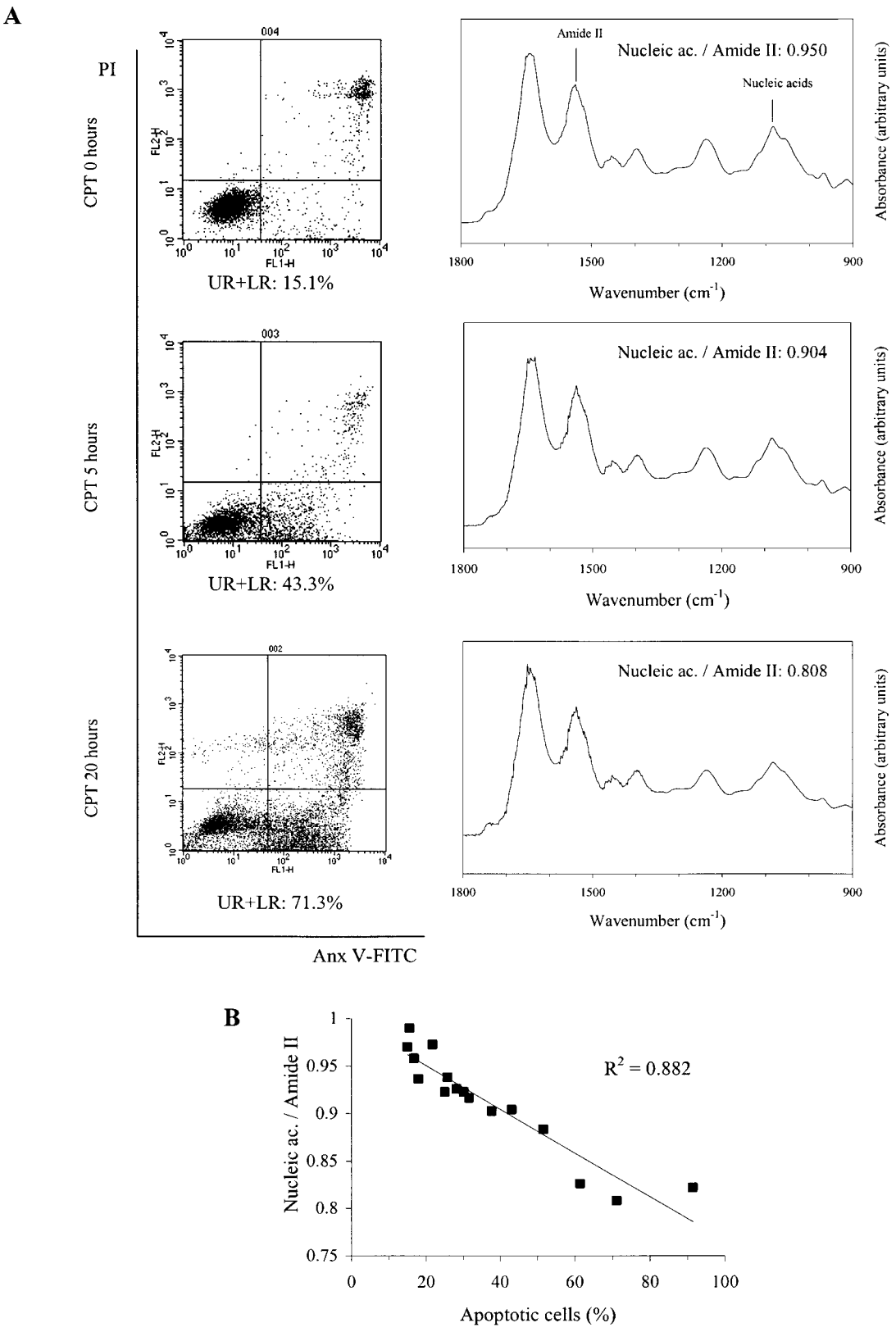

Figure 3 Induction of apoptosis (Anx V-positive cells) and the decrease in the nucleic acids (nucleic ac.)/amide II ratio effected by camptothecin (CPT), showing that the apoptotic index is inversely correlated with the nucleic acids/amide II ratio

(**A**) Flow-cytometry analysis of Anx V/PI-stained cells after treatment with 4 μM camptothecin for different time periods. The corresponding ATR–FTIR spectra are shown on the right. 'UR + LR' refers to the sum of the events acquired in the upper right quadrant (late apoptotic/necrotic cells) and in the low right quadrant (early apoptotic cells) divided by the total number of events acquired in each dot plot. (**B**) Statistical correlation between the nucleic acids/amide II ratio and the apoptosis index (analysis performed from five independent experiments).

selective discrimination between necrotic and apoptotic cells. Further work will clarify the biological meaning of the appearance of this band in the IR spectra of necrotic cells.

CH_2/CH_3 ratio increases during cell growth

To determine whether cell growth conditions affected IR spectra, the ATR–FTIR spectra of HL60 cells were acquired during different growth stages. The growth of HL60 cell cultures (starting from a concentration of 6×10^4 cells/ml, and progressing to 2.5×10^6 cells/ml) was monitored by measuring the cell number and the apoptotic index by nuclear morphological analysis (Figures 2A and 2B). A constant number of cells from the same cultures (3×10^6/sample) was collected every 24 h, and analysed by IR spectroscopy.

We analysed the ratio between the signal in the area 2900–2944 cm^{-1} (assigned to the absorption of CH_2 groups) and that in the area 2945–2980 cm^{-1} (assigned to CH_3): an increase in the CH_2/CH_3 ratio was observed during cell growth in a single culture (Figure 2C). However, the apoptotic index only slightly increased after 120 h (from baseline levels to approx. 10 %), which corresponded to a stable cellular concentration of about 2.5×10^6 cells/ml; at this time point, the cells had already reached the plateau phase of growth. The increase in the CH_2/CH_3 ratio was statistically significant, and reproducible over a large number of HL60 cultures (Figure 2D). It was noteworthy that the CH_2/CH_3 ratio in apoptotic cells did not reveal any significant change with respect to viable cells (see Figure 5B). On the other hand, within the range of cellular concentrations that we investigated, the nucleic acids (region 1000–1140 cm^{-1}) did not significantly change during cell growth, supporting further the specificity of the observed spectral features (results not shown). These results indicated that the changes observed in the CH_2/CH_3 ratio were influenced by cell growth, and were not specific for apoptosis.

The molecular mechanism underlying the CH_2/CH_3 increase has yet to be elucidated, but it may be related to the generation of lipidic second messengers that regulate cellular growth [34–36], or to a slight decrease in cellular volume following extensive growth conditions [37,38]. Indeed, a decrease in the cellular volume corresponds to a relative increase in the surface area. This may cause an augmentation of the phospholipids fraction in the biomass, corresponding to a major enrichment in CH_2 relative to CH_3 groups.

DNA/protein ratio is inversely correlated with the apoptotic index

An analysis of the observed changes in the nucleic acids compared with protein content after apoptosis induction was conducted. To meet this aim, the ratio between the signal in the area 1000–1140 cm^{-1} (assigned to nucleic acids) and that in the area 1483–1595 cm^{-1} (amide II) was measured following the treatment of HL60 cells with increasing concentrations of camptothecin over different time points. The nucleic acids/amide II ratio was then compared with the apoptotic index, as calculated by two different standard methods: Anx V–FITC/PI staining and nuclear morphological analysis.

HL60 cells were treated with 4 μM camptothecin for 5 to 20 h, and analysed for apoptosis induction by flow cytometry after Anx V staining. In parallel, cells were subjected to FTIR-spectroscopic analysis; representative results are shown in Figure 3. Untreated cells contain a baseline population of Anx V-positive cells that varies between 8 and 15 % (in this specific experiment; see also Figure 6); the apoptotic index increased to 43 % after 5 h treatment with camptothecin, and to 71 % after 20 h treatment. Corresponding FTIR spectra show a progressive decrease in the nucleic acids/amide II ratio after 5 and 20 h of treatment with camptothecin. As shown in Figure 3(B), the results obtained from five independent experiments show that the decrease in the nucleic acids/amide II ratio correlates with the apoptotic index, with a significant linear correlation index ($r^2 = 0.882$).

HL60 cells were treated for 20 h with increasing concentrations of camptothecin, and analysed by either nuclear morphology or FTIR spectroscopy. Representative photomicrographs of HL60 cells, after staining with DAPI are shown in Figure 4(A). Untreated cells ('Ctrl'; see the legend to Figure 4) have normal, well-defined and round nuclei; in contrast, nuclei of apoptotic cells appear typically condensed and fragmented into nuclear apoptotic bodies (shown by arrowheads in Figure 4A). The apoptotic index was calculated after morphological analysis and scoring (Figure 4B). The ATR–FTIR spectra in the region 900–1600 cm^{-1} corresponding to the experiments shown in Figure 4(A) are illustrated in Figure 4(C): they are shown overlapped and normalized over the amide II band for the purposes of clarity. Spectral analysis showed that increasing concentrations of camptothecin resulted in a significant decrease in the overall intensity of the nucleic acids region (Figure 5A). The nucleic acids/amide II ratio conformed to a dose–response curve that reached a minimum value of approx. 0.82 at camptothecin doses of between 1 and 4 μM (Figure 5A). To confirm the specificity of these spectral changes, the CH_2/CH_3 ratio of the same FTIR spectra was also measured (Figure 5B): no significant changes after camptothecin treatment, within the concentration ranges that were considered, were observed.

Finally, HL60 cells were treated either with 4 μM camptothecin in DMSO or with DMSO alone for different time points; apoptosis induction was confirmed by nuclear morphological observations (results not shown). We performed a parallel time-course IR analysis on these same cultures: as shown in Figure 5(C), the nucleic acids/amide II ratio decreased over time in treated cells only, thus confirming that the observed FTIR spectral changes, as well as the apoptotic index, followed a time-dependent course. The results from three independent dose–response experiments were plotted against the percentage of apoptotic cells obtained by nuclear morphological analysis (Figure 5D): the nucleic acids/amide II ratio was inversely correlated with the apoptotic index ($r^2 = 0.943$).

Treatment with a caspase inhibitor inhibits FTIR spectral changes associated with apoptosis

To confirm that the observed FTIR spectral changes specifically depend on the execution of early apoptotic events, such as caspase cleavage and activation, we treated HL60 cells for 20 h with 4 μM camptothecin either alone or together with 50 μM Z-VAD-fmk, a potent inhibitor of caspases [39]. The apoptotic index of treated and untreated cells was then assessed by nuclear morphological analysis and by Anx V–FITC/PI staining (Figure 6A). In untreated cells, as well as in cells treated with Z-VAD-fmk, the apoptotic index range varied between 5 and 15 %, depending on the assay used. The apoptotic index increased following treatment with camptothecin, from baseline levels to values exceeding 90 % (nuclear morphology) or 60 % (Anx V–FITC/PI staining), but it was maintained at values lower than 10 % or 20 % respectively in cells treated with camptothecin and Z-VAD-fmk (Figure 6A), confirming that Z-VAD-fmk inhibited camptothecin-induced apoptosis.

In order to confirm further that the apoptosis inhibition was due to specific inhibition of caspase activation, we analysed

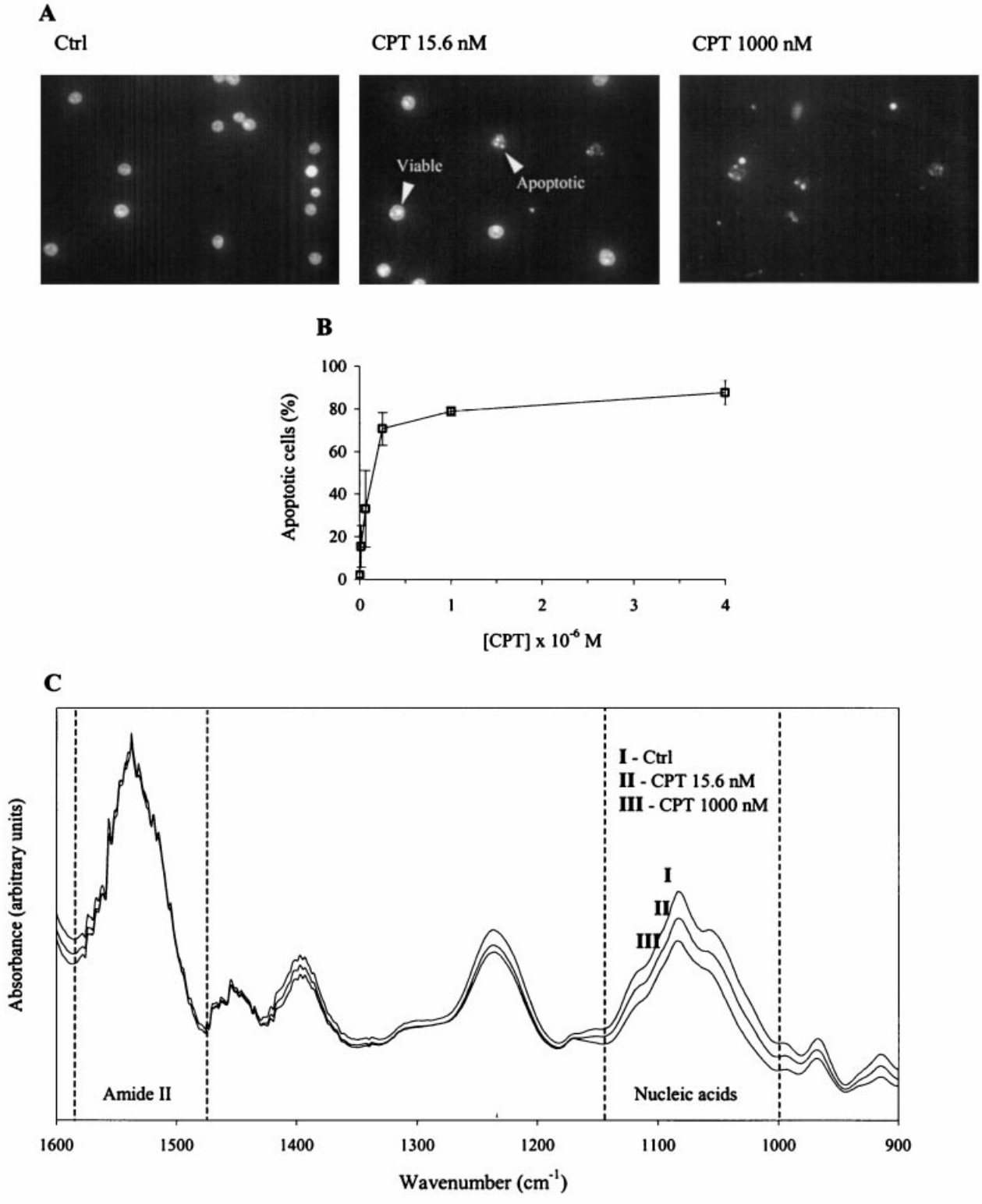

Figure 4 Induction of typical apoptotic nuclear morphology and a decrease in the nucleic acids/amide II ratio effected by camptothecin (CPT)

(**A**) Representative fluorescence microphotographs of untreated HL60 cells (Ctrl), cells treated with 15.6 nM CPT or 1000 nM CPT for 20 h (DAPI staining, objective 40 ×). (**B**) Dose–response curve of the apoptotic index calculated by nuclear morphology analysis (values shown are the means ± S.D. for three independent experiments). (**C**) ATR–FTIR spectra corresponding to the fluorescence microphotographs shown in Figure 4(A). IR spectra of control (Ctrl) cells (**I**), cells treated with 15.6 nM CPT (**II**) and 1000 nM CPT (**III**) are overlapped and normalized over the amide II band. The amide II area and the region assigned to DNA (the 'nucleic acids'-labelled area) are defined by two dotted lines.

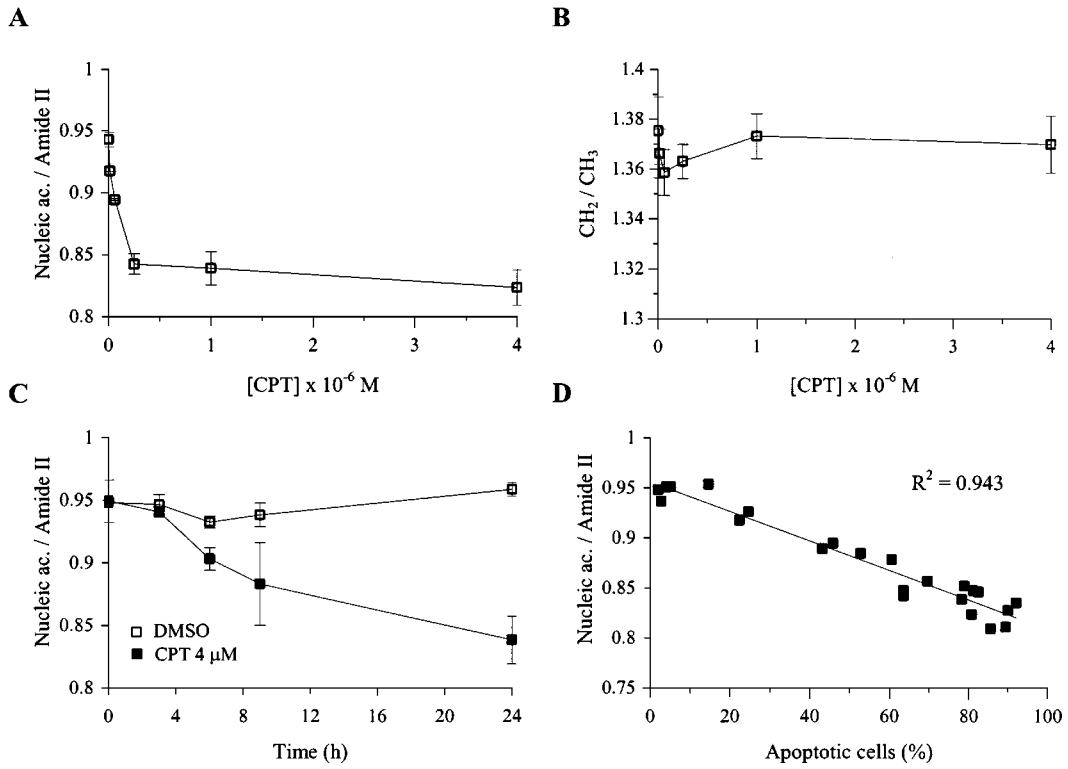

Figure 5 Correlation between the apoptotic index, calculated by nuclear morphology analysis, and a decrease in the nucleic acids/amide II ratio

(**A**) Dose–response curve of the nucleic acids/amide II ratio (values shown are the means ± S.D. for three independent experiments). (**B**) Dose–response curve of the CH_2/CH_3 ratio (values are the means ± S.D. for three independent experiments). (**C**) Time-course analysis of the nucleic acids/amide II ratio with or without 4 μM camptothecin (values are the means ± S.D. for three independent experiments). (**D**) Statistical correlation between the apoptotic index, as assessed by morphological analysis, and the nucleic acids/amide II ratio (the data correspond to the dose–response experiments). CPT, camptothecin.

caspase-3 and PARP cleavage by Western blotting on HL60 soluble proteic extracts. Caspase-3, caspase-6 and caspase-7 are the so-called 'effector' caspases: these are responsible for the events leading to the morphological changes typical of apoptosis. Once the cell is committed to apoptosis, caspase-3 zymogen (32 kDa) undergoes self-cleavage, or is cleaved by other caspases, into two fragments that possess the proteolytic activity. We observed that the band of caspase-3 at 32 kDa decreased in intensity following treatment with camptothecin, but this effect was partially protected following treatment with camptothecin + Z-VAD-fmk (Figure 6B).

PARP is a 116 kDa protein substrate of caspases, which detects and signals DNA-strand breaks [40]. During apoptosis, PARP undergoes poly-ADP-ribosylation, and is cleaved into two fragments of 89 kDa and 24 kDa [41]: PARP cleavage is therefore a specific marker of effector caspases activation. We performed a Western blot analysis using anti-PARP antibodies that recognize both the intact form at 116 kDa and the 89 kDa fragment. As shown in Figure 6(B), in control and in Z-VAD-fmk-treated cells PARP was not cleaved, but the 89 kDa band appeared following treatment with camptothecin. PARP cleavage was prevented in cells treated with camptothecin and Z-VAD-fmk, confirming that effector caspase activity was inhibited by Z-VAD-fmk.

The ATR–FTIR spectra of the same HL60 cells were collected and analysed in triplicate: the nucleic acids/amide II ratio was 0.95 in both untreated and Z-VAD-fmk-treated cells (Figure 6C). The ratio decreased to 0.82 in camptothecin-treated cells, but it was maintained over 0.9 in HL60 cells treated with camptothecin and Z-VAD-fmk. These results confirm that the nucleic acids/amide II ratio depends on caspase activation, and therefore is a specific spectral marker of apoptosis.

Concluding remarks

Here we report that the apoptotic index calculated by two distinct assays was statistically correlated with the apoptotic index, as calculated by the nucleic acids/amide II ratio from FTIR spectroscopy. From these observations, it is evident that FTIR spectroscopy was able to detect a decrease in the overall DNA spectral response in the cells: this may be due to the fact that apoptotic cells fragment their nuclear DNA into regular internucleosomal fragments that eventually may not be recognized as genomic DNA. In addition to this, we also propose that the decrease in absorption in the region 1000–1140 cm^{-1} during apoptosis may be explained by taking into consideration the 'black dot' theory that was recently proposed by Diem and coworkers [24]. Briefly, they analysed using FTIR spectroscopy leukaemia cells in different cell-cycle phases (G_1, S and G_2), and found that spectra of cells in G_1 and G_2 phases were surprisingly similar in the nucleic acids region, even though cells in G_2 have twice the DNA content. Furthermore, cells in S phase presented a remarkable increase in DNA content in the same region with respect to cells in both G_1 and G_2 phases. They explained this phenomenon by hypothesizing that DNA in G_1/G_2 cells was only partly visible, owing to chromatin packing, and concluded

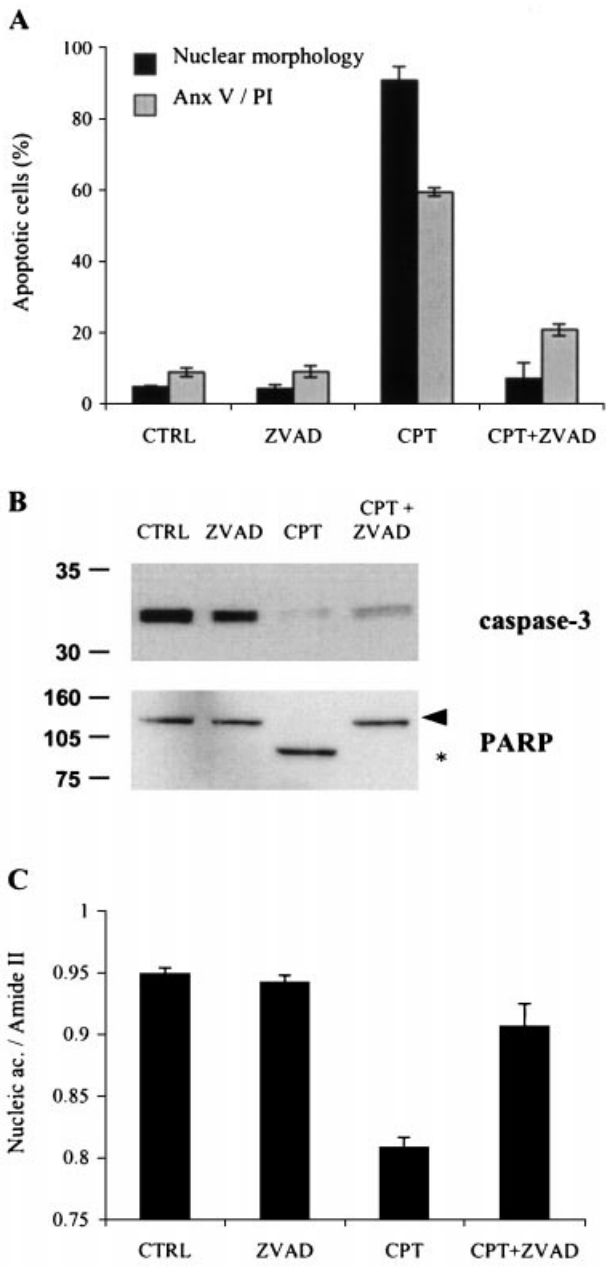

Figure 6 Z-VAD-fmk inhibits FTIR spectral changes associated to camptothecin-induced apoptosis in HL60 cells

(**A**) Apoptotic index from nuclear morphology or Anx V–FITC/PI staining (means ± S.D. for three independent experiments) of HL60 cells not treated (CTRL) or treated for 20 h with 50 μM Z-VAD-fmk (ZVAD), 4 μM camptothecin (CPT) or both (CPT + ZVAD). (**B**) Western blot of HL60-cell extracts corresponding to the experiments shown in (**A**) stained with anti-(caspase-3) or anti-PARP antibodies (the arrowhead and the asterisk indicate the intact form and cleaved fragment of 89 kDa respectively). The positions of molecular mass markers (kDa) are indicated on the left-hand side. (**C**) Nucleic acids/amide II ratio calculated from FTIR spectra of HL60 cells corresponding to (**A**) and (**B**). The means ± S.D. for three independent experiments are shown.

that the condensed chromatin appears to be 'black' to IR spectroscopy, and provides less spectral information because of very high local absorptions. Likewise, we propose that chromatin condensation occurring during apoptosis may lead to a very high increase in absorption of DNA in apoptotic bodies, thus resulting in only a partial visibility of the nucleic acids band on FTIR spectroscopy.

Recently, contradictory reports on differences in the DNA/protein ratio as analysed by FTIR have been published [14,15]. The ATR technique reported here enhances the intensity of bands in the 1800–900 cm^{-1} region due to a major penetration depth of the standing wave at lower, relative to higher, frequencies [13]. This intrinsic characteristic of ATR makes it suitable to detect slight changes in bands assigned to proteins and nucleic acids in the spectral region below 1800 cm^{-1} without requiring complex mathematical analysis. By using the ATR technique, we have obtained results very similar to Mantsch and co-workers [15]. The fact that we have used a different cell line and a different apoptotic stimulus supports further the hypothesis that changes within this area are significantly correlated with the intrinsic apoptotic process, and not with the cell or drug used. Furthermore, we provided clear-cut evidence that the specific inhibition of caspases also prevented the spectral changes related to apoptosis. Importantly, we have compared spectra of apoptotic and necrotic cells for the first time, and detected a specific marker of necrosis that was not present into apoptotic cells.

The IR spectra of intact cells provide both qualitative and quantitative information concerning the overall protein, lipid and nucleic acid content of viable, necrotic or apoptotic cells within a single experimental point, without manipulation or staining of the sample. We therefore propose that this is a novel technical approach to use for monitoring apoptosis induction of human leukaemic cells.

We thank C. Albanese and P. Cappella for assistance in flow-cytometry analysis, and C. Santocanale, J. Bischoff, G. Draetta and R. Bravo for helpful suggestions and discussion. F.G. is supported by a PhD scholarship from the University of Milano-Bicocca.

REFERENCES

1 Cohen, J. J. (1993) Apoptosis Immunol. Today **14**, 126–130
2 Nicholson, D. W., Ali, A., Thornberry, N. A., Vaillancourt, J. P., Ding, C. K., Gallant, M., Gareau, Y., Griffin, P. R., Labelle, M., Lazebnik, Y. A. et al. (1995) Identification and inhibition of the ICE/CED-3 protease necessary for mammalian apoptosis. Nature (London) **376**, 37–43
3 van Engeland, M., Nieland, L. J., Ramaekers, F. C., Schutte, B. and Reutelingsperger, C. P. (1998) Annexin V-affinity assay: a review on an apoptosis detection system based on phosphatidylserine exposure. Cytometry **31**, 1–9
4 Wyllie, A. H. (1980) Glucocorticoid-induced thymocyte apoptosis is associated with endogenous endonuclease activation. Nature (London) **284**, 555–556
5 Gavrieli, Y., Sherman, Y. and Ben Sasson, S. A. (1992) Identification of programmed cell death *in situ* via specific labeling of nuclear DNA fragmentation. J. Cell Biol. **119**, 493–501
6 Willingham, M. C. (1999) Cytochemical methods for the detection of apoptosis. J. Histochem. Cytochem. **47**, 1101–1109
7 Martin, S. J., Finucane, D. M., Amarante-Mendes, G. P., O'Brien, G. A. and Green, D. R. (1996) Phosphatidylserine externalization during CD95-induced apoptosis of cells and cytoplasts requires ICE/CED-3 protease activity. J. Biol. Chem. **271**, 28753–28756
8 Griffiths, P. R. and de Haseth, J. A. (1986) Fourier Transform Infrared Spectrometry. John Wiley and Sons, New York
9 Diem, M., Boydston-White, S. and Chiriboga, L. (1999) Infrared spectroscopy of cells and tissues: shining light onto a novel subject. Appl. Spectrosc. **53**, 148–161
10 Rigas, B., Morgello, S., Goldman, I. S. and Wong, P. T. (1990) Human colorectal cancers display abnormal Fourier-transform infrared spectra. Proc. Natl. Acad. Sci. U.S.A. **87**, 8140–8144
11 Cohenford, M. A. and Rigas, B. (1998) Cytologically normal cells from neoplastic cervical samples display extensive structural abnormalities on IR spectroscopy: implications for tumor biology. Proc. Natl. Acad. Sci. U.S.A. **95**, 15327–15332
12 Schultz, C. P., Liu, K. Z., Kerr, P. D. and Mantsch, H. H. (1998) *In situ* infrared histopathology of keratinization in human oral/oropharyngeal squamous cell carcinoma. Oncol. Res. **10**, 277–286
13 Goormaghtigh, E., Raussens, V. and Ruysschaert, J. M. (1999) Attenuated total reflection infrared spectroscopy of proteins and lipids in biological membranes. Biochim. Biophys. Acta **1422**, 105–185

14 Zhou, J., Wang, Z., Sun, S., Liu, M. and Zhang, H. (2001) A rapid method for detecting conformational changes during differentiation and apoptosis of HL60 cells by Fourier-transform infrared spectroscopy. Biotechnol. Appl. Biochem. **33**, 127–132
15 Liu, K. Z., Jia, L., Kelsey, S. M., Newland, A. C. and Mantsch, H. H. (2001) Quantitative determination of apoptosis on leukemia cells by infrared spectroscopy. Apoptosis **6**, 269–278
16 Kaufmann, S. H. (1989) Induction of endonucleolytic DNA cleavage in human acute myelogenous leukemia cells by etoposide, camptothecin, and other cytotoxic anticancer drugs: a cautionary note. Cancer Res. **49**, 5870–5878
17 Del Bino, G. and Darzynkiewicz, Z. (1991) Camptothecin, teniposide, or 4′-(9-acridinylamino)-3-methanesulfon-m-anisidide, but not mitoxantrone or doxorubicin, induces degradation of nuclear DNA in the S phase of HL-60 cells. Cancer Res. **51**, 1165–1169
18 Bertrand, R., Solary, E., Jenkins, J. and Pommier, Y. (1993) Apoptosis and its modulation in human promyelocytic HL-60 cells treated with DNA topoisomerase I and II inhibitors. Exp. Cell. Res. **207**, 388–397
19 Casiano, C. A., Ochs, R. L. and Tan, E. M. (1998) Distinct cleavage products of nuclear proteins in apoptosis and necrosis revealed by autoantibody probes. Cell Death Differ. **5**, 183–190
20 Pevsner, A. and Diem, M. (2001) Infrared spectroscopic studies of major cellular components. Part I: the effect of hydration on the spectra of proteins. Appl. Spectrosc. **55**, 788–793
21 Pevsner, A. and Diem, M. (2001) Infrared spectroscopic studies of major cellular components. Part II: the effect of hydration on the spectra of nucleic acids. Appl. Spectrosc. **55**, 1502–1505
22 Savitzky, A. and Golay, M. J. (1964) Smoothing and differentiation of data by simplified least squares procedures. Anal. Chem. **36**, 1627–1639
23 Benedetti, E., Bramanti, E., Papineschi, F., Rossi, I. and Benedetti, E. (1997) Determination of the relative amount of nucleic acids and proteins in leukemic and normal lymphocytes by means of Fourier transform infrared microspectroscopy. Appl. Spectrosc. **51**, 792–797
24 Boydston-White, S., Gopen, T., Houser, S., Bargonetti, J. and Diem, M. (1999) Infrared spectroscopy of human tissue. Infrared spectroscopic studies of myeloid leukemia (ML-1) cells at different phases of the cell cycle. Biospectroscopy **5**, 219–227
25 Goormaghtigh, E., Cabiaux, V. and Ruysschaert, J. M. (1994) Determination of soluble and membrane protein structure by Fourier transform infrared spectroscopy. Secondary structures. Subcell. Biochem. **23**, 405–450
26 Surewicz, W. K. and Mantsch, H. H. (1988) New insight into protein secondary structure from resolution-enhanced infrared spectra. Biochim. Biophys. Acta **952**, 115–130
27 Schultz, C. P., Liu, K., Johnston, J. B. and Mantsch, H. H. (1996) Study of chronic lymphocytic leukemia cells by FT-IR spectroscopy and cluster analysis. Leukemia Res. **20**, 649–655
28 Dixit, V. M. (1996) Role of ICE-proteases in apoptosis. Adv. Exp. Med. Biol. **406**, 113–117
29 Garrido, C., Gurbuxani, S., Ravagnan, L. and Kroemer, G. (2001) Heat shock proteins: endogenous modulators of apoptotic cell death. Biochem. Biophys. Res. Commun. **286**, 433–442
30 Xanthoudakis, S. and Nicholson, D. W. (2000) Heat-shock proteins as death determinants. Nat. Cell Biol. **2**, 163–165
31 Jesenberger, V. and Jentsch, S. (2002) Deadly encounter: ubiquitin meets apoptosis. Nat. Rev. Mol. Cell. Biol. **3**, 112–121
32 Goossens, J. F., Henichart, J. P., Dassonneville, L., Facompre, M. and Bailly, C. (2000) Relation between intracellular acidification and camptothecin-induced apoptosis in leukemia cells. Eur. J. Pharm. Sci. **10**, 125–131
33 Tamm, L. and Tatulian, S. A. (1997) Infrared spectroscopy of proteins and peptides in lipid bilayers. Q. Rev. Biophys. **30**, 365–429
34 Jamin, N., Dumas, P., Moncuit, J., Fridman, W. H., Teillaud, J. L., Carr, G. L. and Williams, G. P. (1998) Highly resolved chemical imaging of living cells by using synchrotron infrared microspectrometry. Proc. Natl. Acad. Sci. U.S.A. **95**, 4837–4840
35 Spiegel, S. (1999) Sphingosine 1-phosphate: a prototype of a new class of second messengers. J. Leukocyte Biol. **65**, 341–344
36 Cantrell, D. A. (2001) Phosphoinositide 3-kinase signalling pathways. J. Cell Sci. **114**, 1439–1445
37 McDowell, C. L. and Papoutsakis, E. T. (1998) Decreasing extracellular pH increases CD13 receptor surface content and alters the metabolism of HL60 cells cultured in stirred tank bioreactors. Biotechnol. Prog. **14**, 567–572
38 McDowell, C. L. and Papoutsakis, E. T. (1998) Serum increases the CD13 receptor expression, reduces the transduction of fluid-mechanical forces, and alters the metabolism of HL60 cells cultured in agitated bioreactors. Biotechnol. Bioeng. **60**, 259–268
39 Dolle, R. E., Hoyer, D., Prasad, C. V., Schmidt, S. J., Helaszek, C. T., Miller, R. E. and Ator, M. A. (1994) P1 aspartate-based peptide α-((2,6-dichlorobenzoyl)oxy)methyl ketones as potent time-dependent inhibitors of interleukin-1 β-converting enzyme. J. Med. Chem. **37**, 563–564
40 Herceg, Z. and Wang, Z. Q. (2001) Functions of poly(ADP-ribose) polymerase (PARP) in DNA repair, genomic integrity and cell death. Rev. Mutat. Res. **477**, 97–110
41 Tewari, M., Quan, L. T., O'Rourke, K., Desnoyers, S., Zeng, Z., Beidler, D. R., Poirier, G. G., Salvesen, G. S. and Dixit, V. M. (1995) Yama/CPP32 β, a mammalian homolog of CED-3, is a CrmA-inhibitable protease that cleaves the death substrate poly(ADP-ribose) polymerase. Cell **81**, 801–809

Received 1 July 2002/16 October 2002; accepted 16 October 2002
Published as BJ Immediate Publication 16 October 2002, DOI 10.1042/BJ20021021